Development and characterization of rigid polyester blends for 4D printing

Jose Gonzalez [2,3]; Gamaliel H. Martinez[2,3]; Benjamin Estrada[1,3]; Katia Lizbeth Delgado Ramos[1,3]; Jose F. Salazar[1,3]; Brian E. Schuster[2,3]; David A. Roberson[1,3,*]

1. Polymer Extrusion Lab, The University of Texas at El Paso, El Paso TX, 79968
2. Dynamic Materials Laboratory, The University of Texas at El Paso, El Paso TX, 79968
3. Department of Metallurgical, Materials and Biomedical Engineering, The University of Texas at El Paso, El Paso, TX 79968

* Corresponding Author: droberson@utep.edu

Abstract

Incorporating thermoplastic materials with shape memory properties into the fused filament fabrication process enables what is commonly referred to as 4D printing. When the blends are composed of one or more materials with inherent shape memory properties, the tailoring of critical parameters such as shape recovery temperature can be realized. Previous work by our group demonstrated the creation of shape memory polymer blends where one component was elastomeric. The following work entails the development and characterization of rigid polyester blends that are biocompatible and biodegradable in addition to having shape memory properties. Dynamic mechanical analysis (DMA) was used to determine the critical deformation and recovery temperatures. The effect of print raster patterns on the DMA results was also evaluated. Micro-tensile testing was used to characterize the physical properties of the materials at elevated temperatures. Finally, scanning electron microanalysis was used to examine the fracture surfaces of spent tensile specimens.

Keywords: 4D Printing, Shape memory polymers, Digital image correlation, Fused filament fabrication

Introduction

Shape memory polymers (SMP)s add another dimension to the manufacturing method of 3D printing to the point that integration of this material class with the fabrication technique has been coined as "4D printing." SMPs have the capability to return to their original shape when deformed, through an external stimulus such as heat, light, electricity, among others (Barletta *et al.*, 2021).

Strategies for the development of novel shape memory materials can fall into two categories: 1) the creation of polymer composites; and 2) the creation of polymer blends. Examples can be found in materials development of SMP composites in the biomedical field where filler materials including carbon nanotubes, carbon nanofibers, and graphene have been added to enhance shape memory materials (Zhao *et al.*, 2019). Polymer blending has also been found to be beneficial, again using work in the biomedical field as an example, the addition of polycaprolactone (PCL) to polylactic acid (PLA) has been shown to be beneficial due to a lowering of the acidity of PLA (Ebrahimi and Ramezani Dana, 2022). We note here the PLA and PCL are both commonly used 3D printing feedstock materials commonly used in the fused filament fabrication (FFF) process and they are both SMPs. The combination of FFF and SMPs allows for

the design of structures engineered to self-assemble at precise locations and shapes increasing the applicability of digital manufacturing (González-Henríquez *et al.*, 2019).

Polyester materials with shape memory properties have been explored by our group and others due to their biocompatibility as well as an ability to be incorporated as feedstock materials for the additive manufacturing (AM) process of FFF. Common polyesters include PLA, PCL, and thermoplastic urethane (TPU). For example, Barletta, et al. investigated the shape memory properties of FFF-made cellular structures composed of PLA that was modified by the addition of 10% by mass TPU (Barletta *et al.*, 2021). Work by Rahmatabadi et al. explored aspects such as infill (raster) pattern on the shape memory properties of PLA/TPU blends (Rahmatabadi *et al.*, 2024). Ma, et al. explored the 4D printing of blends composed of PLA and PCL where the PCL content was varied in order to tailor the glass transition temperature (T_g) of the resultant blend, thus controlling the critical shape memory recovery temperature (Ma *et al.*, 2021). Another work by Liu et al. (Liu *et al.*, 2023) characterized the 4D printing of PLA and PLA/PCL blends and applied a neural network algorithm to optimize the aspects of shape programming and found this optimization to enhance the shape memory properties.

Specific to previous work performed by our group, we characterized the shape memory performance of the PLA/TPU blend system and also characterized the resultant phase morphology by way of scanning transmission electron microscopy (STEM) (Quiñonez *et al.*, 2021). This previous study by Quiñonez et al. also noted that the shape memory properties for FFF-made specimens were greater than those observed for injection molded specimens, a phenomena associated with the AM process aligning the phases (Chávez *et al.*, 2018; Quiñonez *et al.*, 2021). Work by Carrillo et al. explored the shape memory properties of binary blends composed of PCL and TPU and a ternary blend composed of equal parts by mass PCL, TPU, and PLA and also noted a strengthening effect caused by the shape deformation and recovery cycle (Carrillo *et al.*, 2024).

A common methodology for assessing shape memory properties is the determination of the shape recovery ratio (R_r) and the shape fixation ratio (R_f) where the typical process is as follows (Chávez *et al.*, 2018; Lai and Lan, 2013; Yang *et al.*, 2016): 1) a tensile test specimen is typically deformed under stress to 100% elongation (ε_m) at a temperature just below T_g; 2) the specimen is then allowed to cool and removed from the tensile test machine and the length of the specimen is then measured (ε_u); and 3) finally, the specimen is recovered for a duration of time under heat at a temperature above T_g and the length of the recovered specimen is measured (ε_p). The $R_r$and R_f are then calculated by the following equations:

$$R_r = \frac{\varepsilon_m - \varepsilon_p}{\varepsilon_m} X\ 100\% \qquad (1),$$

$$R_f = \frac{\varepsilon_u}{\varepsilon_m} X\ 100\% \qquad (2)$$

A perceived drawback to this method of measuring the shape memory properties of polymers in the method described above is the need for a tensile tester with a temperature-controlled chamber. There are several alternatives to the typical methods for the calculation of $R_r$and R_f values. One method demonstrated by Yu et al. (Yu *et al.*, 2019) employed the use of a beam structure that was folded in half to a temporary (fixed) shape and then recovered to the permanent shape; where the angles of the folded and recovered structures provided the measurements used to calculate the shape memory properties as follows:

$$R_r = \frac{\theta_{max} - \theta_i}{\theta_{max}} X\ 100\% \qquad (3),$$

$$R_f = \frac{\theta_{fixed}}{\theta_{max}} X\ 100\%, \qquad (4)$$

where θ_{max} is the maximum angle of folding, θ_{fixed} is the measured angle after the load is removed from the folded structure, and θ_i is the angle measured after recovery. This method provides a way to achieve measurements of critical shape memory properties when deformation at an elevated temperature is necessitated.

The work presented here explores the characterization of PLA and the PLA/PCL blend system where compositions of (by mass) 90/10, 80/20 and 70/30 PLA/ PCL were studied. These two constituents were chosen because they are both long chain polyesters and have similar Hildebrand solubility parameters (δ) with PCL having a value ranging from 15.8 to 21.2 $MPa^{1/2}$ (Adamska *et al.*, 2016) and PLA having a value ranging between 19.9 and 20.7 $MPa^{1/2}$ (Su *et al.*, 2020). The similarities in polymer structure and solubility parameters led to the expectation that the resultant blends would be miscible without the need for compatibilizers. A simplistic method for the determination of the shape memory values was conducted that allowed for the deformation of the specimens at an elevated temperature without the need for specialized equipment. In contrast, characterization of the deformation and recovery process was also carried out with a micro tensile tester using digital image correlation (DIC)-aided micro tensile testing.

Experimental Procedure

The PLA used in this work was Grade 4043D supplied by Nature Works (NatureWorks, LLC, Minnetonka MN, USA) The PCL used in this work was obtained from Polly Plastics (Midland, MI, USA). Both materials were obtained in the form of pellets. The pellets were first dried using a compressed air dryer (Micro Dryer CAFM station, Dri-Air Industries, East Windsor, CT, USA). Compositions of PLA and PCL were melt compounded using a Collin twin screw extruder/compounder (Model ZK 21T, Collin Lab and Pilot Solutions, Norcross, GA, USA). The compounder was equipped with a melt pump and a belt puller to facilitate extrusion of a filament compatible with the FFF printer used in this study (a filament with a target diameter of 2.85mm). The extrusion parameters are listed in Table 1.

Table 1. Extrusion and printing parameters for the materials studied here.

Extruder Parameters	Zone 1	175°C
	Zone 2	180°C
	Zone 3	180°C
	Zone 4	180°C
	Zone 5	175°C
	Zone 6	175°C
	Pressure 1	90 Bar
	Extruder screws	10 RPM
	Melt Pump screws	12 RPM
	Melt Pump pressure	5 Bar
Print Parameters	Print Temperature	210°C
	Bed Temperature	60°C

Two FFF printers were used in this study. For the fabrication of tensile test specimens and specimens for DMA a Lulzbot Taz 5 (Fargo Additive Manufacturing Equipment, Fargo, ND, USA) outfitted with a single extruder with a 0.5mm print nozzle. The geometry of the tensile test specimens was in accordance with ASTM D638 Type IV dimensions, while the dimensions for the DMA measured 30 X 9 X 3 mm. the tensile specimens were fabricated in a longitudinal raster pattern where the print rasters were parallel to the length of the specimen. Specimens for DMA were fabricated in two raster patterns, one longitudinal and the other transverse, where the print rasters were perpendicular to the length of the specimen. Specimens for use on the micro tensile tester were fabricated with a Lulzbot Taz Workhorse FFF printer also with a 0.5mm print nozzle. The geometry of this specimen type was custom for the instrument used which was a Psylotech micro tensile tester (Psylotech, Evanston, Illinois, USA). Examples of printed test specimens are seen in Figure 1. The DMA used was a Perkin Elmer DMA 8000 (Perkin Elmer, Waltham, MA, USA). The tensile test machine used was an MTS Criterion C.44 (MTS, Eden Prairie, MN, USA) tensile tester with an Advantage Model AHX 800 high elongation extensometer.

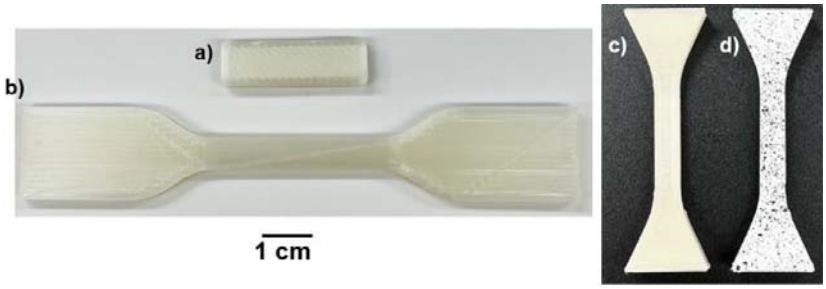

Figure 1. Examples of a) a printed DMA specimen, b) a Tupe IV tensile specimen, c) a micro tensile specimen, and d) a micro tensile specimen that has been painted with speckles for digital image correlation.

For the determination of the shape memory parameters of $R_r$and R_f, a beam structure was designed and printed with the TAZ workhorse. The structure was created with a notch to facilitate bending. Specimens were heated for a duration of 5 min at 60 °C in a VWR Signature horizontal air flow oven (Model 1370FM, VWR International, West Chester, PA, USA), folded in half by hand and then allowed to cool. The θ_{fixed} was then measured and the specimens were then recovered at 75 °C in the oven for five minutes. The specimens were allowed to cool to room temperature and then the θ_i was measured. A schematic of this specimen and measuring process is seen in Figure 2.

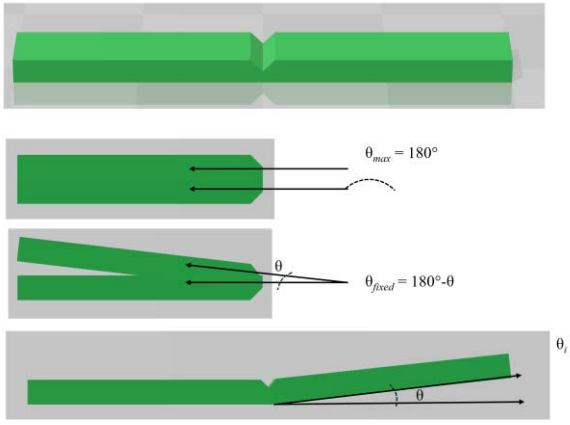

Figure 2. Schematic of the specimen and method used to determine shape memory parameters.

Specimens for micro tensile testing were printed and subsequently coated with white spray paint. Once dried, the samples were speckled with black spray paint applied by flicking the bristles a toothbrush coated with the paint, creating a random and fine dot pattern to ensure precision in DIC data. The specimens' width and thickness were measured initially. Using the Pyslotech micro tensile tester, the tensile sample was loaded into the grips, and the protective window was secured. The sample was preloaded in tension to a minimal force between 0 and 200 newtons.

The "Victory Test" program was then initiated, providing the micro tensile machine with the specifications for heating and straining the tensile sample. The test segments were as follows:

1. Ramp in Drive Control: +5.00E^{-3}m Amplitude, 16.00E^{-6} m/s Speed, Temperature Setpoint 60.0°C, Sampling at 20.000 Hz, Lowpass Filter Cutoff of 100.000 Hz.

2. Hold in Drive Control: 120 seconds, Temperature Setpoint 60.0°C, Sampling at 20.000 Hz, Lowpass Filter Cutoff of 100.000 Hz.

3. Hold in Drive Control: 120 seconds, Temperature Setpoint 38.0°C, Sampling at 20.000 Hz, Lowpass Filter Cutoff of 100.000 Hz.

4. Ramp in Drive Control: -50.00E-6m Amplitude, 1.00E-6 m/s Speed, Temperature Setpoint 38.0°C, Sampling at 20.000 Hz, Lowpass Filter Cutoff of 100.000 Hz.

5. Hold in Drive Control: 180 seconds, Temperature Setpoint 75.0°C, Sampling at 20.000 Hz, Lowpass Filter Cutoff of 100.000 Hz.

Environmental parameters were set to 60°C, and the measurements of the specimens' width and thickness were entered. Upon reaching 60°C, the load and displacement were zeroed. The Correlated Solutions DIC system was used to open the Camera Data Acquisition (DAC) system. The camera's focus and crosshair were aligned, file paths for each system were set, and both systems were started simultaneously. Recovery of the specimens was carried out at 75 °C. Data collection continued until a point post-max recovery was reached, at which time it was stopped.

For post-processing, VIC Snap 2-D, a program within the Correlated Solutions DIC system, was utilized. The speckled images were imported, and a point of interest, encompassing the complete gauge length, was set. The program ran, processing all the images, and correlated the beginning and ending images to obtain strain data in any axis. The information was then exported as CSV Excel files. This process was repeated for all collected samples, including natural PLA, 90/10 PLA/PCL, 80/20 PLA/PCL, and 70/30 PLA/PCL, though for this work we will only present the data from the 70/30 PLA/PCL blend.

Results

As can be seen in Figure 3, the addition of PCL leads to a decrease in ultimate tensile strength (UTS) as compared to PLA alone. Data from prior work with PLA (PA Quiñonez, D Bermudez, L Ugarte-Sanchez, DA Roberson, 2019; Quiñonez *et al.*, 2021) produced specimens that yielded UTS values of 59.9 ± 2.13 MPa. For the blends PLA/PCL 70/30 yielded an average UTS of 13.10 ± 6.77 MPa while the 80/20 composition yielded values of 23.46 ± 5.79 MPa.

Specimens fabricated from 90/10 blend exhibited the highest amount of variability with UTS values of 21.16 ± 15.43 MPa.

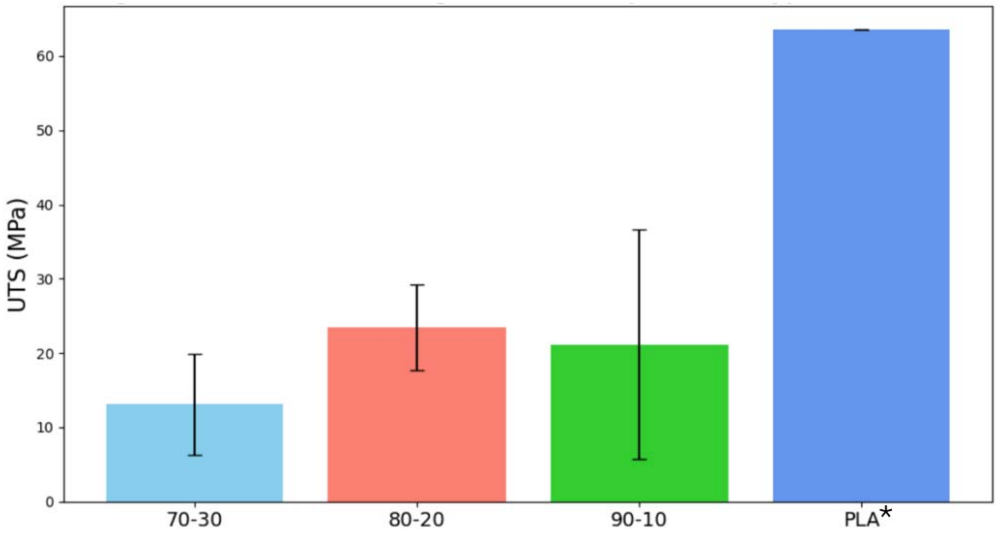

Figure 3. UTS values for PLA and the PLA/PCL blends studied in this work. *Data from (Quiñonez *et al.*, 2021)

Data obtained from the DMA was used to determine the temperatures for deformation and recovery of the PLA and PLA/PCL specimens. Data from previous work with pure PLA (Bermudez *et al.*, 2021) was used as a baseline for comparison with the PLA/PCL blends and is presented in Figure 4. Comparing the two raster patterns shows a difference in the storage modulus curves and a slight difference in the max tan δ values (2.47 for the transversal specimens and 2.63 for the longitudinal specimens). The temperature at which the max tan δ was observed was similar for the two raster patterns curves at 71.75° C for transversal and 70.84 °C for the longitudinal specimens.

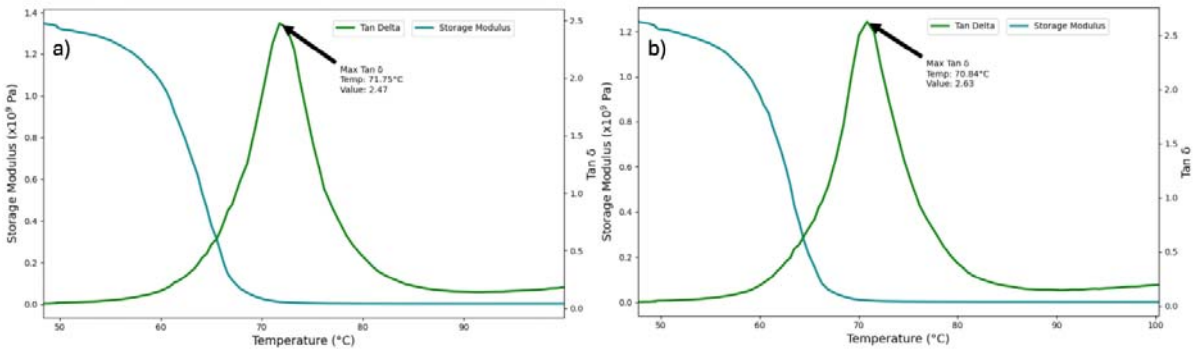

Figure 4. DMA Curves for PLA printed in the a) transversal and b) longitudinal raster patterns. Data from (Bermudez *et al.*, 2021)

Comparison of the curves from the different blend ratios of PLA/PCL shows that an increase of PCL content reduces the dampening characteristics and creates a material with an increase in energy return (Fig. 5.). In the case of the longitudinal raster pattern there is a steady decrease in max tan δ values with an increase in PCL content, however there is not a proportional relationship in the case of the transversal raster pattern. Overall, the blends of PLA/PCL have

lower max tan δ values as compared to PLA. The DMA data provided us with critical information that allowed us to design the shape memory characterization experiments. The relatively similar temperatures for the recording of the max tan δ values (~65°) led to the decision to deform specimens at 60 °C and recover the specimens at 75 °C.

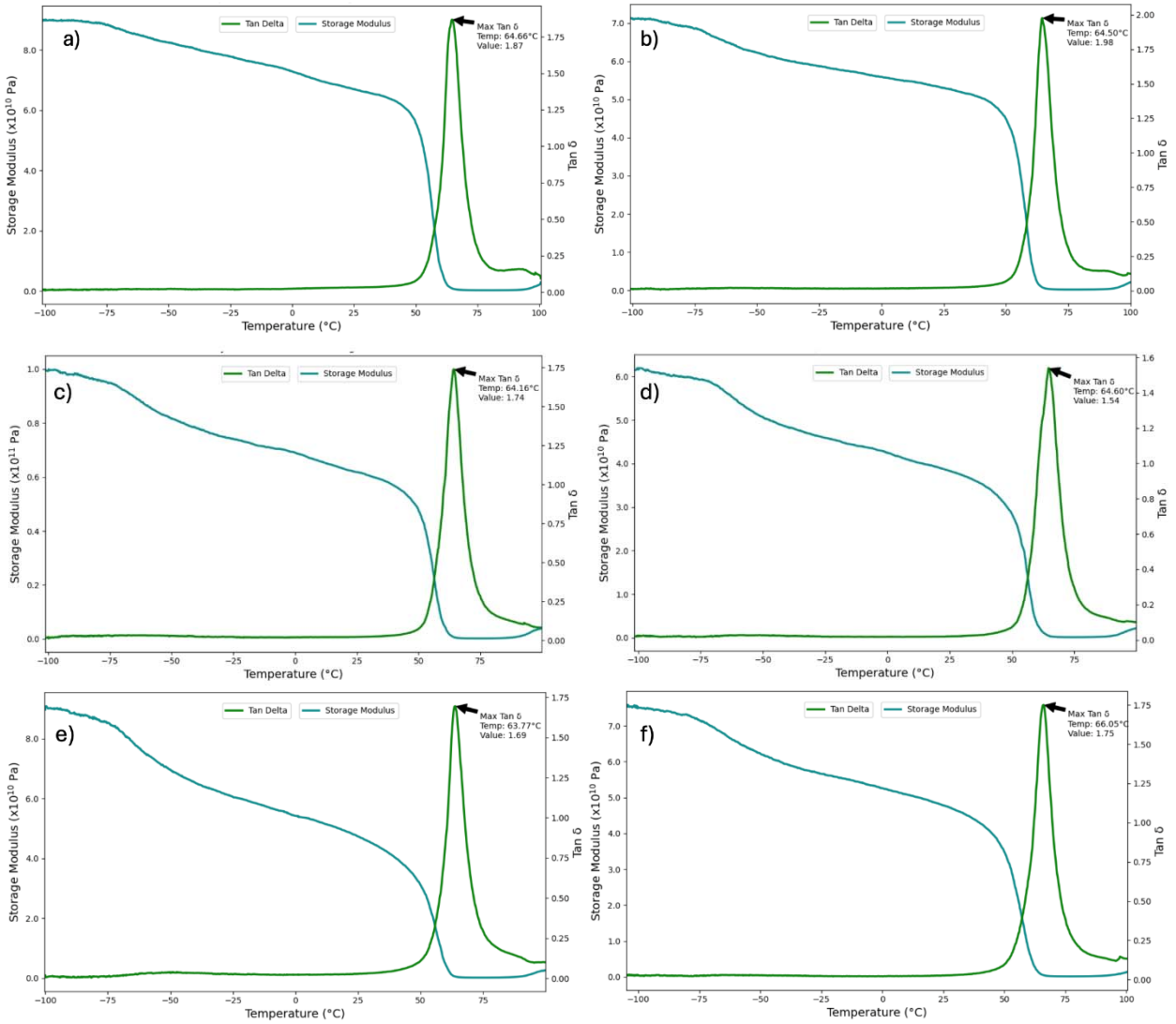

Figure 5. DMA curves of PLA/PCL per blend type 90/10 a) longitudinal, b) transverse; 80/20 c) longitudinal, d) transverse: 70/30 e) longitudinal, f) transverse.

Shape Memory Characterization

Initial characterization of the shape memory properties of the PLA/PCL system were carried out by fabricating small sheets of the different material compositions by FFF. The sheets were heated to a temperature below the max tan δ temperature (60 °C) in an oven and then recovered in water at a temperature of ~75 °C. Stills from a video documenting the recovery process are seen in Figure 6. The observed results were puzzling. The specimens would recover to their original shape, but then curl. This may be indicative of a secondary shape memory response. An example of this is seen in Figure 7c.

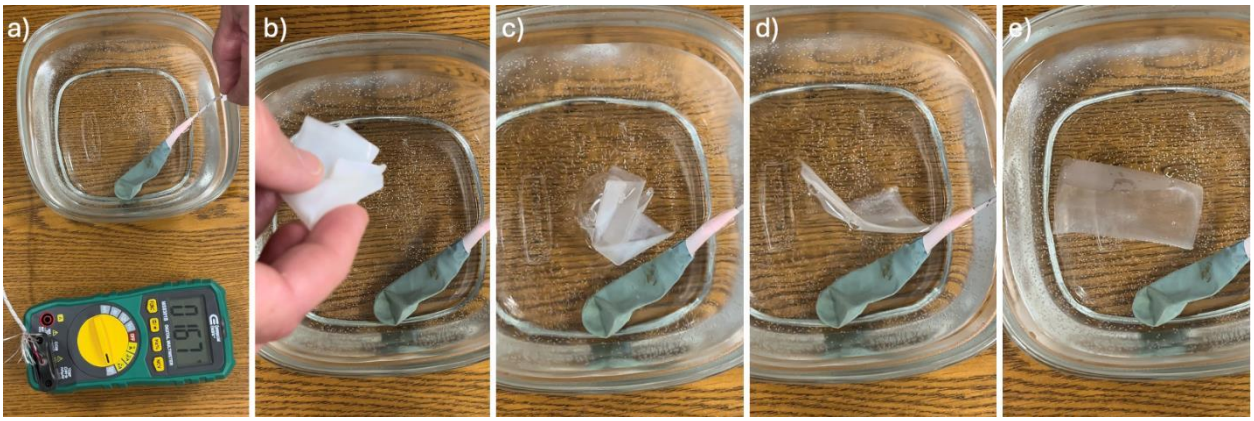

Figure 6. Process of shape memory recovery a) Set temperature at 167 °F (75°C), b) folding shape to insert on water, c) Initiation 1, d) 2s, and e) After 3s recovery successfully.

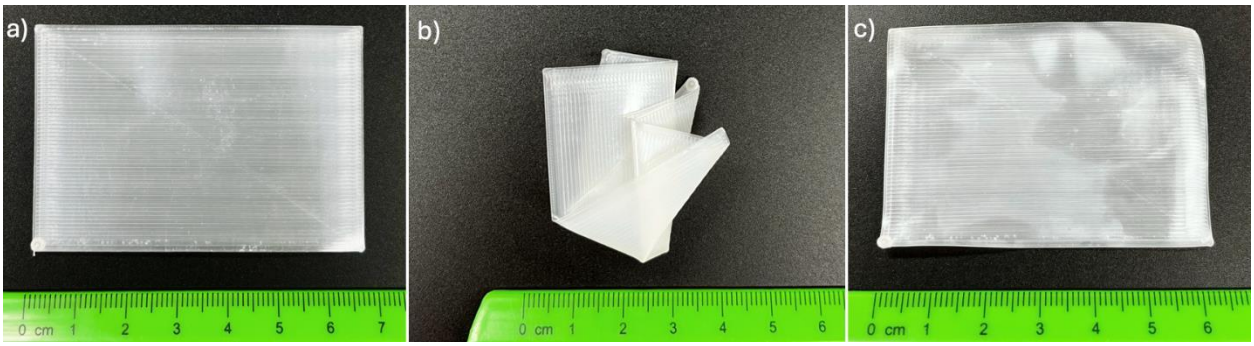

Figure 7. The stages of an initial shape memory experiment where a) is the initial as-printed shape, b) is the specimen after deformation at 60 °C, and c) is the specimen after recovery in water at 75 °C.

An example of the determination of the critical shape memory properties by way of the beam specimen is seen in Figures 8 and 9. Most of the samples had similar behavior, as was the case will all other shape memory characterization experiments specimens were deformed at 60 °C and recovered at 75°C. As was the case with the sheet specimen described above, curling of the beam specimen also occurred making measurement of the critical angles difficult. We note here that all specimens opened up to the original angle during recovery making the R_r for all materials studied here 100%.

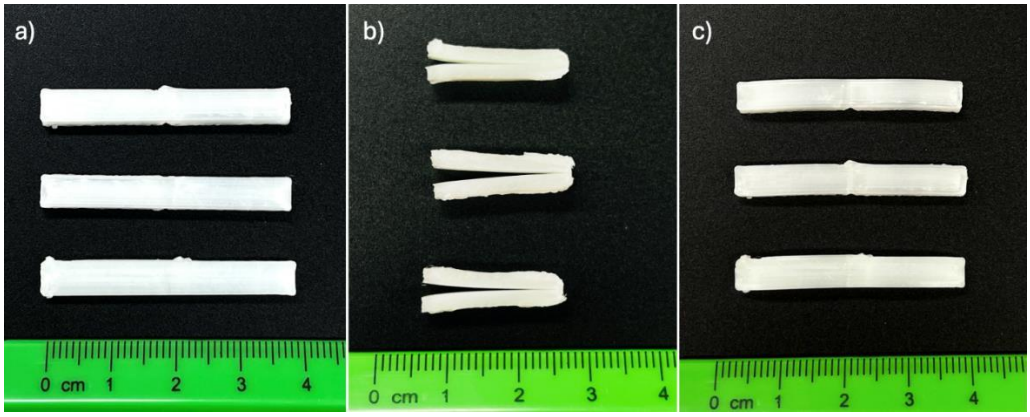

Figure 8. Shape memory polymer thermal process a) initial shape, b) deformed condition, and c) recovered shape.

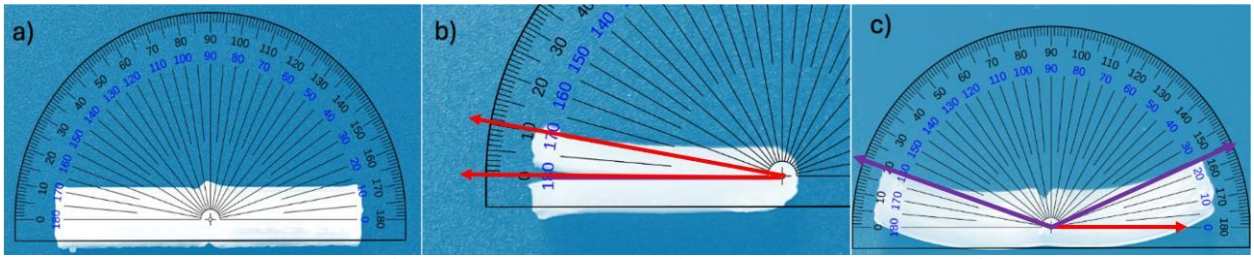

Figure 9. Visual representations of calculating the angles of shape memory polymer a) as-printed condition b) angle used to calculate θ_{fixed}, and c) angle used to calculate θ_i. The purple arrows indicate curvature caused by a secondary shape memory effect.

Though the behavior of the specimen convoluted the ability to obtain precise measurements needed to calculate the critical shape memory parameters, the methodology did allow us to determine that the blends of PLA and PCL possess tangible shape memory properties. The PCL content did not significantly affect the shape memory properties as compared to pure PLA. This behavior may have been predictable due to the similarities in glass transition temperature among the blend systems as observed by DMA. The calculated shape memory properties are tabulated in Table 2.

Table 2. R_r and R_f values.

BLEND	n	R_f	R_r
PURE PLA	3	89.2 ± 0.01	100
90-10	3	86.6 ± 3.0	
80-20	3	88.8 ±1.1	
70-30	1	88.8	

Images obtained from DIC analysis are seen in Figure 10 starting with the end of the deformation cycle and ending during the recovery cycle. As can be seen the specimen is recovering to its original shape as the cycle goes on. The heat map indicates levels of stress while the red dashed line has been included to aid in the discernment of the shape recovery process.

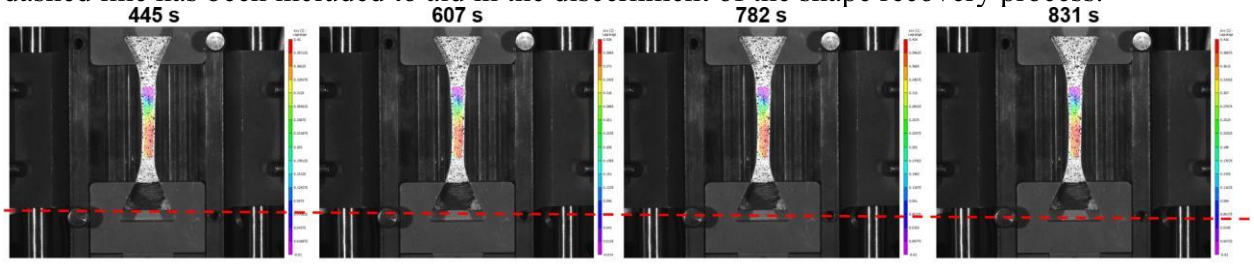

Figure 10. DIC images of a portion of the shape memory cycle for a specimen composed of the 70/30 PLA/PCL blend.

The plots for this cycle are seen in Figure 11, made from data for the same 70/30 PLA/PCL specimen. The process can be analyzed featuring three stacked graphs, each illustrating different parameters: temperature, displacement, and load. All tables share time as the x-axis value. The first table presents the temperature data over time, showcasing how the thermal properties of the blend change during the experiment. The temperature measurements are critical for understanding the thermal stability and behavior of the PLA/PCL blend under varying conditions. The second table displays the displacement data over time. This data is essential for evaluating the mechanical response of the blend when subjected to stress. It provides insights into the deformation characteristics and helps in understanding the material's elasticity and plasticity. The third table

illustrates the load data over time, which indicates the amount of force applied to the blend during testing. This information is crucial for determining the blend's load-bearing capacity and its ability to withstand mechanical stress. By analyzing these three sets of data concurrently, we can gain a comprehensive understanding of the 70/30 PLA/PCL blend's performance. The correlation between temperature, displacement, and load over time allows for a detailed assessment of the material's behavior under various conditions, aiding in the optimization and application of this polymer blend in 4-D printing.

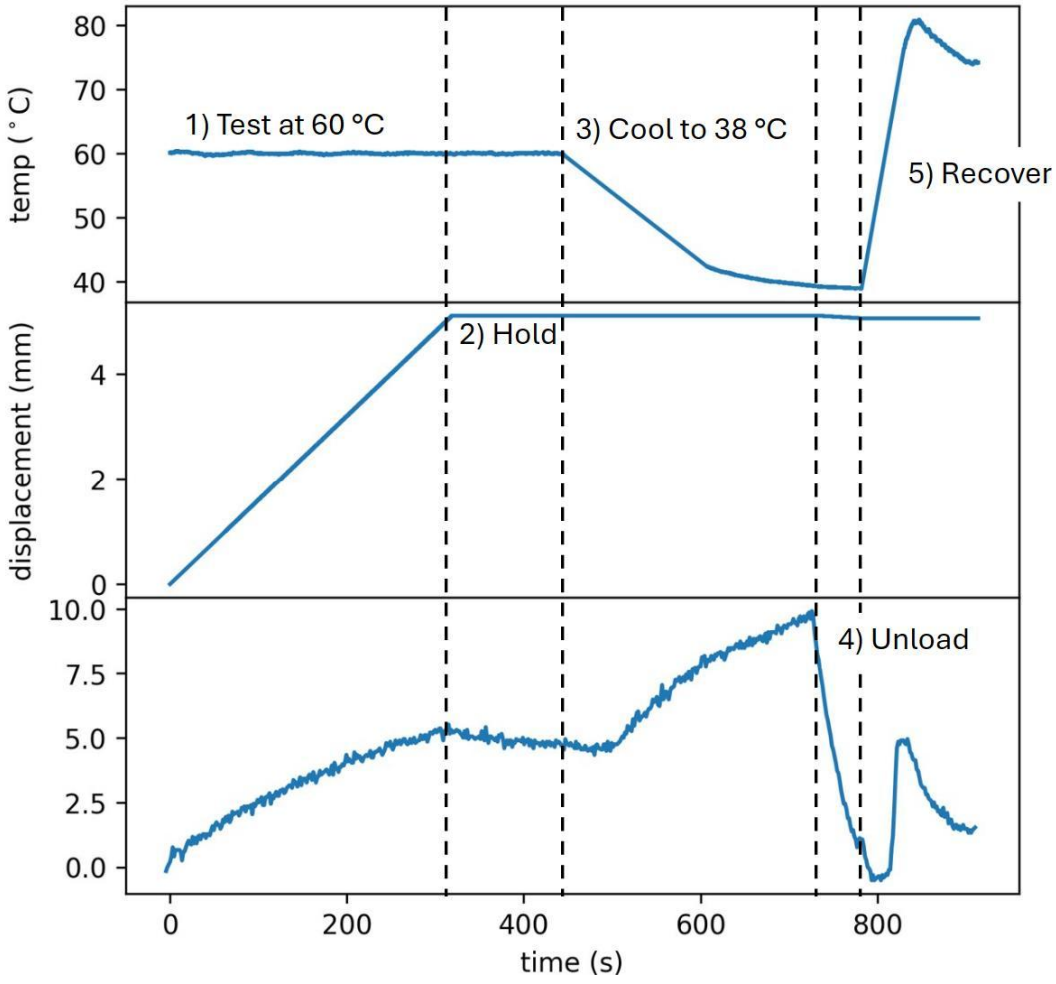

Figure 11. DIC data for a 70/30 PLA/PCL Blend

The DIC data for a 70/30 PLA/PCL blend can be analyzed by examining the testing process: heating to 60°C, holding at that temperature, cooling to 38°C, unloading, and recovering. Initially, heating to 60°C records temperature data to understand the material's thermal behavior and identify significant changes. During the hold period, DIC captures stabilization data, assessing structural integrity. Cooling to 38°C monitors contraction and thermal recovery. Unloading records the blend's elasticity and deformation recovery. Finally, the recovery phase observes the blend's return to its baseline state, providing insights into long-term durability and resilience. As can be seen from the load strain curve of the deformation and recovery process in Figure 12, the recovery process exerts a load of ~5N on the specimen grips.

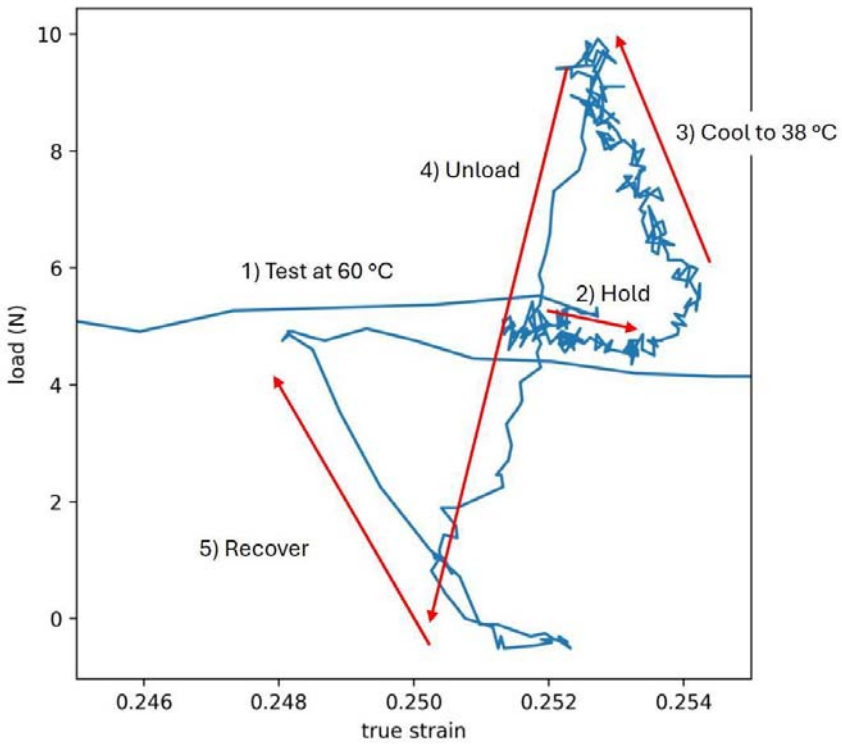

Figure 12. Load/Strain curve for a 70/30 PLA/PCL specimen subjected to a deformation/recovery cycle.

We point out here that though the DIC-aided analysis provides more information pertaining to the shape memory cycle, a drawback to this methodology is that the specimen does not fully recover as seen in Fig 13. The lack of full recovery is most-likely caused by the holding of the specimen in the grips of the instrument. Though the traditional parameters cannot be calculated from this data, aspects related to the shape recovery process such as the relative energy exerted by the material during the recovery process can be discerned, making this a valuable aspect of the characterization of shape memory properties. Moreover, no curling of the DIC specimens was observed, increasing the validity of the collected data as compared to our other efforts in quantifying the shape memory properties of the PLA/PCL blend system in the case of FFF-made specimens.

Figure 13. Comparison of an as-printed DIC specimen with one that was subjected to the shape memory cycle.

Fracture Surface Analysis

Analysis of the fracture surfaces of spent tensile specimens revealed that all material systems exhibited a brittle fracture mode. Beginning with the PLA (Fig. 14a), the fracture surface morphology is indicative of craze cracking associated with a brittle failure mode (Bermudez *et al.*, 2021; Perez *et al.*, 2014). A fibril (highlighted by the white arrow in Fig. 14a) was also present. An example specimen from the 90/10 PLA/PCL blend sample pool (Fig. 14b) also exhibited a fracture surface indicative of a brittle fracture mode driven by craze cracking. Again, a fibril was observed (indicated by the white arrow). The blend specimen composed of the mass ratio of 80/20 PLA/PCL (Fig. 14c) exhibited a somewhat higher level of ductile fracture surface features with a larger number of fibrils and a qualitatively higher degree of plastic deformation, though the overall fracture surface morphology was dominated by craze cracking. Finally, the fracture surface of the 70/30 PLA/PCL blend (Fig. 14d) also exhibited a brittle fracture mode, however, with a more planar morphology indicating that this composition was the most brittle, in agreement with the tensile test data.

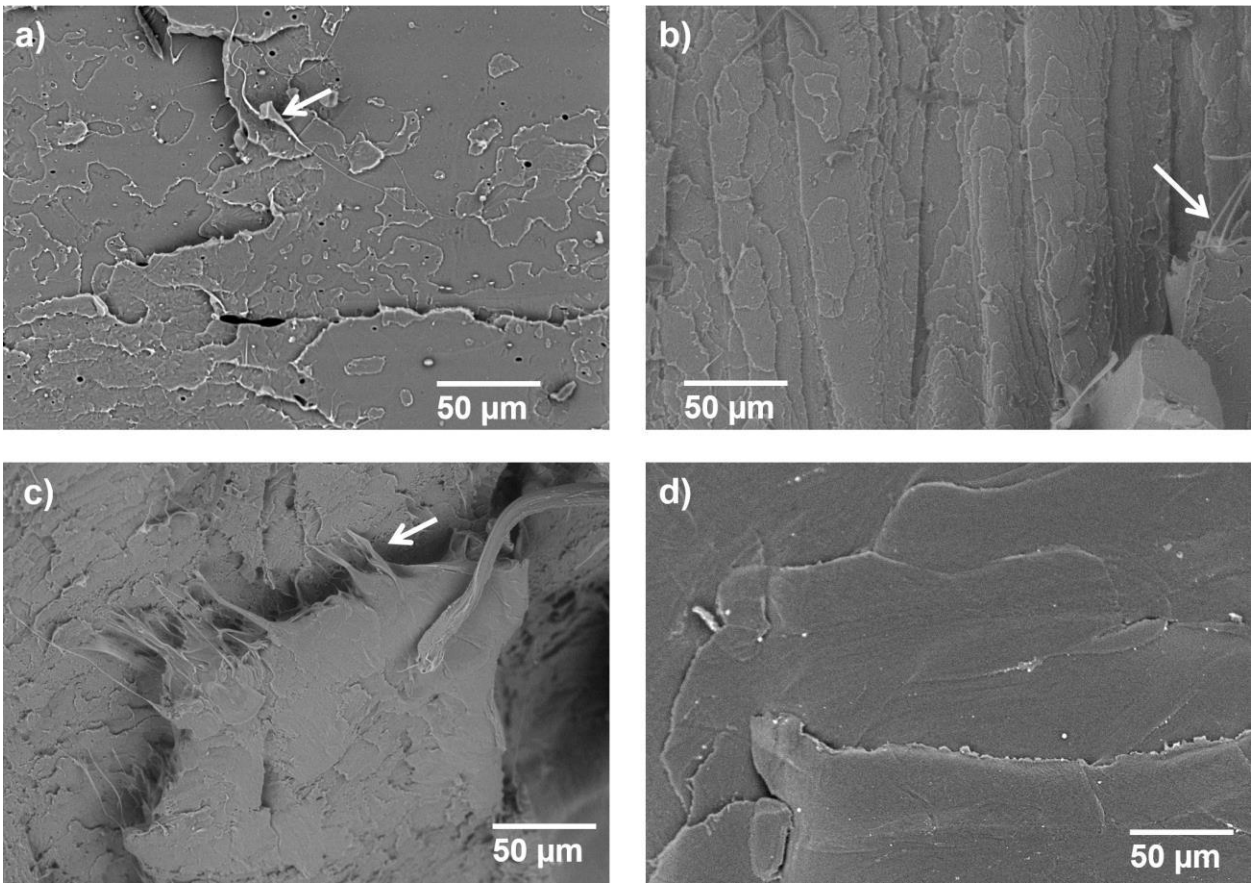

Figure 14. SEM images of the fracture surface of a) PLA, b) PLA/PCL 90/10, c) PLA/PCL 80/20, and d) PLA/PCL 70/30.

Conclusions and Future Work

Characterization of the PLA/PCL blend system was problematic due to the curling of the specimens during the elevated temperature deformation and recovery processes. Even so the ability to gain some quantifiable insight into the shape memory properties of this blend system where specimens are deformed at elevated temperatures was still valuable. Integration of DIC-assisted

tensile testing provides a wider range of information pertaining to the shape recovery process as compared to more traditional methods where the calculation of R_r and R_f by way of tensile testing has been the norm.

Future work includes completion of the DIC analysis for the other blend systems as well as a comparison of print raster patterns. The goal of this is to understand if the alignment of the print rasters has an effect on the exerted energy of the specimens during the recovery process. In past efforts we have shown that multi-component shape memory polymer systems contain distinct phases that are aligned by the FFF process and that this alignment has an effect on shape memory properties (Chávez *et al.*, 2018).

The work presented here demonstrated the combination of simple and complex characterization methodologies for shape memory feedstock materials for AM. A key to the advancement of AM is the incorporation of advanced material systems. As the demands for higher-functioning material systems increase, the need for a broad spectrum of materials characterization techniques becomes paramount.

Acknowledgements.

The work presented here was performed in the Polymer Extrusion Lab and the Dynamic Materials Laboratory, both in the Department of Metallurgical, Materials and Biomedical Engineering (MMBME) at The University of Texas at El Paso (UTEP). The authors acknowledge support provided by the Consortium of Hybrid Resilient Energy Systems (CHRES), which is funded by the Department of Energy, Office of Science under award number DE-NA0003982. This work was also supported by Los Alamos National Laboratory under agreement number SPN01166, Techsource, Inc. under agreement SPN1858 and Northrop Gruman under agreement SPN01858. Funding was also provided by the National Science Foundation (NSF) under grant number CMMI 2227573.

References

Adamska, K., Voelkel, A. and Berlińska, A. (2016), "The solubility parameter for biomedical polymers—Application of inverse gas chromatography", *Journal of Pharmaceutical and Biomedical Analysis*, Vol. 127, pp. 202–206, doi: 10.1016/j.jpba.2016.04.014.

Barletta, M., Gisario, A. and Mehrpouya, M. (2021), "4D printing of shape memory polylactic acid (PLA) components: Investigating the role of the operational parameters in fused deposition modelling (FDM)", *Journal of Manufacturing Processes*, Vol. 61, pp. 473–480, doi: 10.1016/j.jmapro.2020.11.036.

Bermudez, D., Quiñonez, P.A., Vasquez, E.J., Carrete, I.A., Word, T.J. and Roberson, D.A. (2021), "A Comparison of the physical properties of two commercial 3D printing PLA grades", *Virtual and Physical Prototyping*, Taylor & Francis, Vol. 16 No. 2, pp. 178–195, doi: 10.1080/17452759.2021.1910047.

Carrillo, L.E.L., Gonzalez, Y.O., Parga, M., Ramos, K.L.D., Neparko, N. and Roberson, D.A. (2024), "Development of binary and ternary polyester shape memory blends for additive manufacturing", *Journal of Materials Science*, Vol. 59 No. 18, pp. 8040–8057, doi: 10.1007/s10853-024-09657-7.

Chávez, F.A., Siqueiros, J.G., Carrete, I.A., Delgado, I.L., Ritter, G.W. and Roberson, D.A. (2018), "Characterisation of phases and deformation temperature for additively manufactured shape memory polymer components fabricated from rubberised

acrylonitrile butadiene styrene", *Virtual and Physical Prototyping*, Vol. 0 No. 0, pp. 1–15, doi: 10.1080/17452759.2018.1550694.

Ebrahimi, F. and Ramezani Dana, H. (2022), "Poly lactic acid (PLA) polymers: from properties to biomedical applications", *International Journal of Polymeric Materials and Polymeric Biomaterials*, Taylor & Francis, Vol. 71 No. 15, pp. 1117–1130, doi: 10.1080/00914037.2021.1944140.

González-Henríquez, C.M., Sarabia-Vallejos, M.A. and Rodriguez-Hernandez, J. (2019), "Polymers for additive manufacturing and 4D-printing: Materials, methodologies, and biomedical applications", *Progress in Polymer Science*, Vol. 94, pp. 57–116, doi: 10.1016/j.progpolymsci.2019.03.001.

Lai, S.-M. and Lan, Y.-C. (2013), "Shape memory properties of melt-blended polylactic acid (PLA)/thermoplastic polyurethane (TPU) bio-based blends", Journal of Polymer Research, Vol. 20 No. 5, p. 140, doi: 10.1007/s10965-013-0140-6.

Liu, Z., Gao, P., Wu, Q., Wang, Z., Li, J., Wang, K., Li, G., et al. (2023), "4D printing of PLA/PCL composites with tunable shape memory properties via printing and programming parameters", *Smart Manufacturing*, World Scientific Publishing Co., p. 2350001, doi: 10.1142/S2737549823500011.

Ma, S., Jiang, Z., Wang, M., Zhang, L., Liang, Y., Zhang, Z., Ren, L., *et al.* (2021), "4D printing of PLA/PCL shape memory composites with controllable sequential deformation", *Bio-Design and Manufacturing*, Vol. 4 No. 4, pp. 867–878, doi: 10.1007/s42242-021-00151-6.

PA Quiñonez, D Bermudez, L Ugarte-Sanchez, DA Roberson. (2019), "Tailoring Physical Properties of Shape Memory Polymers for FDM-type Additive Manufacturing", *Solid Freeform Fabrication 2019: Proceedings of the 30th Annual International Solid Freeform Fabrication Symposium – An Additive Manufacturing Conference*, presented at the 30th Annual International Solid Freeform Fabrication Symposium – An Additive Manufacturing Conference, The University of Texas at Austin, Austin, TX USA, pp. 843–855.

Perez, A.R.T., Roberson, D.A. and Wicker, R.B. (2014), "Fracture Surface Analysis of 3D-Printed Tensile Specimens of Novel ABS-Based Materials", *Journal of Failure Analysis and Prevention*, Vol. 14 No. 3, pp. 343–353, doi: 10.1007/s11668-014-9803-9.

Quiñonez, P.A., Ugarte-Sanchez, L., Bermudez, D., Chinolla, P., Dueck, R., Cavender-Word, T.J. and Roberson, D.A. (2021), "Design of Shape Memory Thermoplastic Material Systems for FDM-Type Additive Manufacturing", *Materials*, Multidisciplinary Digital Publishing Institute, Vol. 14 No. 15, p. 4254, doi: 10.3390/ma14154254.

Rahmatabadi, D., Soltanmohammadi, K., Aberoumand, M., Soleyman, E., Ghasemi, I., Baniassadi, M., Abrinia, K., *et al.* (2024), "4D printing of porous PLA-TPU structures: effect of applied deformation, loading mode and infill pattern on the shape memory performance", *Physica Scripta*, IOP Publishing, Vol. 99 No. 2, p. 025013, doi: 10.1088/1402-4896/ad1957.

Su, S., Duhme, M. and Kopitzky, R. (2020), "Uncompatibilized PBAT/PLA Blends: Manufacturability, Miscibility and Properties", Materials, Multidisciplinary Digital Publishing Institute, Vol. 13 No. 21, p. 4897, doi: 10.3390/ma13214897.

Yang, Y., Chen, Y., Wei, Y. and Li, Y. (2016), "3D printing of shape memory polymer for functional part fabrication", *The International Journal of Advanced Manufacturing Technology*, Vol. 84 No. 9–12, pp. 2079–2095, doi: 10.1007/s00170-015-7843-2.

Yu, Z., Wang, Z., Li, H., Teng, J. and Xu, L. (2019), “Shape Memory Epoxy Polymer (SMEP) Composite Mechanical Properties Enhanced by Introducing Graphene Oxide (GO) into the Matrix”, *Materials*, Multidisciplinary Digital Publishing Institute, Vol. 12 No. 7, p. 1107, doi: 10.3390/ma12071107.

Zhao, W., Liu, L., Zhang, F., Leng, J. and Liu, Y. (2019), “Shape memory polymers and their composites in biomedical applications”, *Materials Science and Engineering: C*, Vol. 97, pp. 864–883, doi: 10.1016/j.msec.2018.12.054.